Struct Multidisc Optim (2012) 45:529–543
DOI 10.1007/s00158-011-0711-2

RESEARCH PAPER

Classification approach for reliability-based topology optimization using probabilistic neural networks

Jiten Patel · Seung-Kyum Choi

Received: 27 March 2010 / Revised: 22 August 2011 / Accepted: 24 August 2011 / Published online: 27 September 2011

Abstract This research explores the usage of classification approaches in order to facilitate the accurate estimation of probabilistic constraints in optimization problems under uncertainty. The efficiency of the proposed framework is achieved with the combination of a conventional topology optimization method and a classification approach-namely, probabilistic neural networks (PNN). Specifically, the implemented framework using PNN is useful in the case of highly nonlinear or disjoint failure domain problems. The effectiveness of the proposed framework is demonstrated with three examples. The first example deals with the estimation of the limit state function in the case of disjoint failure domains. The second example shows the efficacy of the proposed method in the design of stiffest structure through the topology optimization process with the consideration of random field inputs and disjoint failure phenomenon, such as buckling. The third example demonstrates the applicability of the proposed method in a practical engineering problem.

Keywords Reliability-based topology optimization · Probabilistic neural network · Uncertainty · Classification approach

1 Introduction

In the field of structural optimization, designers are often faced with situations where the underlying structural response is either discontinuous or highly nonlinear. The discontinuities may occur due to numerous critical points (limit or bifurcation points) in the system response, such as in cases of buckling, bistable material behavior, nonlinear transient dynamic problems, etc. This presents a challenge to designers since most of the gradient based optimization procedures cannot be used in this situation due to the discontinuity and nonlinearity in the system behavior. Classification approaches can be useful for the reliability analysis in the case of the discontinuous or disjoint failure problems (Hurtado and Alvarez 2003; Basudhar et al. 2008). The classifier is trained to recognize and identify a data point based on whether the data point leads to a safe design or an unsafe design. Hence, unlike the regression process, the classification process does not require the evaluation of the performance function. This makes the classification approach highly effective in the case of a disjoint failure domain where most of the regression based procedures fail to predict the performance function because of the discontinuous nature of the failure domain. Significant research work has been done in this research area for developing efficient classification methods such as Artificial Neural Networks (Hornik 1991), decision trees (Brown et al. 1993; Curram and Mingers 1994), discriminant analysis (Patwo et al. 1993; Curram and Mingers 1994), CART (Atlas et al. 1990; Dietterich and Bakiri 1995), k-nearest–neighbor (Huang and Lippmann 1987; Patwo et al. 1993), and linear programming (Patwo et al. 1993). Traditional statistical classification procedures such as discriminant analysis and decision trees are built on the Bayesian decision theory (Duda and Hart 1973). In these methods, a probability model must be assumed in order to calculate the posterior probability upon which the classification decision is made (Zhang 2000). Hence, the validity of the underlying assumptions is important for these methods to work properly. A good depth of knowledge in both data property and

J. Patel · S.-K. Choi (✉)
G. W. Woodruff School of Mechanical Engineering,
Georgia Institute of Technology, Atlanta, GA 30332, USA
e-mail: schoi@me.gatech.edu

model capabilities is essential in order to use these methods properly.

Neural networks have emerged as an important tool for classification. Specifically, Artificial Neural Networks (ANNs) are processing devices (algorithms or actual hardware) that are loosely modeled after the neuronal structure of the mammalian cerebral cortex, but on much smaller scales (Curram and Mingers 1994). Various research has proved that ANN's are a promising alternative to conventional classification techniques (Michie et al. 1994). Michie et al. (1994) report a comparative study in which three general classification techniques of neural networks- statistical classifiers and machine learning use 23 techniques on 20 different real data sets. The general conclusion drawn from the study was that no single classifier is the best for all datasets. However, the feed forward and backpropagation ANN's have good performance over a wide range of problems. The advantages of ANN include: 1) ANN can be used as black box models since they are data driven and self-adaptive in nature, 2) ANN has been proved to be able to approximate any function with arbitrary accuracy (Cybenko 1989; Hornik et al. 1989; Hornik 1991), and 3) ANN is able to estimate the posterior probabilities, which provides the basis for estimating classification rules like Bayes classification rule and perform statistical analysis (Richard and Lippmann 1991). Since all classification procedures seek a functional relationship between the independent variable and the feature, these attributes are essential for the success of the classification procedure. Thus, it is easy to model real world data which has nonlinear and complex relationships by utilizing ANN.

Topology optimization is often referred to as layout optimization or generalized shape optimization (Rozvany et al. 1995). For structural topology optimization the structures can be considered as either discrete structures or continuum structures (Bendsøe and Sigmund 2003). For continuum structures the shape of the external and internal boundaries and the number of holes are optimized; whereas, for discrete structures the topology problem is solved by determining the optimum number, the position and the mutual connectivity of structural member elements. For topology optimization of continuum structures the reader is referred to the paper by Bendsøe and Kikuchi (1988) which is a seminal paper in this field. The topology optimization problems considered in this paper are discrete in nature, and an up-to-date account in this area can be found in Rozvany et al. (1995).

Discrete structural topology optimization operates on a fixed mesh of finite elements and defines a design variable, which is associated with each element in the mesh. In these topology optimization problems, the ground-truss/structure can be used, which is a framework of pin-connected truss members which carry only axial loads (Sigmund 1995; Frecker et al. 1997; Kogiso et al. 2008). In the case of ground-truss based topology optimization, the feasible design space can become disjoint if buckling and stress constraints are considered (Sved and Ginos 1968; Zhou 1996; Kirsch 1990). The discontinuity of stress function makes it difficult in traditional topology optimization formulation to insert and remove truss members (Kirsch 1990; Dobbs and Felton 1969). In order to circumvent this problem, we propose the usage of the buckling criteria as a limit state function in the reliability-based optimization procedure. This would eliminate the inherent problems encountered when ground-truss based topology optimization is conducted using buckling or stress constraints.

A deterministic optimization process can be overly designed or lead to catastrophic failure of the system depending upon the selected safety factor based on the designer's preference. This issue was addressed by integrating the uncertainty quantification process into the deterministic design process, i.e., robust design (Tsui 1992) and reliability-based design (Choi et al. 2006). Reliability-based design reduces the probability of failure of the system in case the system is exposed to uncertain forces and boundary conditions. An integrated approach of the reliability analysis and topology optimization procedures, such as reliability-based topology optimization (RBTO), yield structures that are more reliable than those produced by deterministic topology optimization methods (Kharmanda et al. 2004). Maute and Frangopol (2003), applied RBTO to synthesize compliant mechanisms for MEMS base application. The level-set based topology optimization procedure (Wang et al. 2005) has also been combined with stochastic optimization techniques for RBTO (Conti et al. 2008). Chen et al. (2010), investigated the application of random field uncertainty for the robust shape and topology optimization using the level set method. However, realistic representations of uncertainty and the improvement of the computational efficiency are still challenging in the existing methods (Michelle 1904; Tu and Choi 1997). In reliability-based design optimization problems, the designer can be faced with cases where the limit state function is nonlinear or discontinuous. Specifically, the use of classical approaches to assess the probabilities of failure is further limited in the disjoint failure region problems (Basudhar et al. 2008). Thus, the proposed method will overcome this limitation with the disjoint failure problem or discontinuous problems by integrating a novel probability analysis procedure into the RBTO. This research explores the usage of classification approaches, specifically probabilistic neural networks (PNN) (Specht 1990), in order to facilitate the accurate estimation of the probability of failure (P_f) for the RBTO process. A classification-based RBTO framework is proposed for the cases where the limit state functions are discontinuous, disjoint or nonlinear. This proposed

method is shown to be effective in dealing with topology optimization problems with a buckling constraint and the inherent discontinuity in the problem. In the following sections, a brief description of the PNN, RBTO, and a proposed technique will be given. Consequently, the implementation of a classification-based RBTO framework will be discussed which can account for both uncertainty and complexity in objectives and constraints. The applicability and efficacy of the proposed framework is demonstrated with the design of mesostructured material.

2 Probabilistic neural network based classification

Probabilistic neural networks (PNN) have been successfully used for diverse pattern recognition applications such as image recognition, texture recognition, signal processing, finance, and biomedical applications (Chtioui et al. 1997; Wang et al. 1998). The PNN is a pattern classifier that combines the widely used Bayes decision strategy with the Parzen nonparametric estimator (Parzen 1962) for estimation of probability density functions of different classes (Specht 1990). Unlike other neural network architectures, PNN is easy to implement and the network is easily interpretable. Most of the decision rules for classification use "Bayes strategies" in order to reduce the "expected risk" in pattern classification (Richard and Lippmann 1991).

Consider a statistic θ that belongs to either of the two classes θ_A or θ_B. If a decision of whether $\theta = \theta_A$ or $\theta = \theta_B$ has to be made based on the data represented in the p-dimensional vector $X^T = [X_1 X_2 \ldots X_j \ldots X_p]$, the Bayes decision rule is represented by

$$d(x) = \theta_A \quad \text{if} \quad h_A l_A f_A(X) > h_B l_B f_B(X) \tag{1}$$

$$d(x) = \theta_B \quad \text{if} \quad h_A l_A f_A(X) < h_B l_B f_B(X) \tag{2}$$

where $f_A(X)$ and $f_B(X)$ are probability density functions (PDF) for categories A and B, respectively. l_A is the loss function associated with the decision $d(X) = \theta_B$ when $\theta = \theta_A$ and l_B is the loss function associated with the decision $d(X) = \theta_A$ when $\theta = \theta_B$. h_A is the a priori probability of occurrence of patterns from category A and $h_B = 1 - h_A$ is the a priori probability that $\theta = \theta_B$. In general, a quadratic loss function can be used for many classification algorithms. For this scenario the quadratic loss function (Witten and Frank 2005) can be given as

$$l = (h_A - \theta_A)^2 + (h_B - \theta_B)^2 \tag{3}$$

where $l = l_A$ orl_B corresponding to $\theta = \theta_A$ or θ_B. Here, θ can only take values of either 0 or 1. Hence, if $\theta = \theta_A$ then $\theta_A = 1$ and $\theta_B = 0$.

The boundary between the region where the Bayes decision $d(X) = \theta_A$ and the region where $d(X) = \theta_B$ is given by

$$f_A(X) = K f_B(X) \tag{4}$$

$$\text{where} \quad K = \frac{h_B l_B}{h_A l_A} \tag{5}$$

In theory, the decision boundary represented by (4) can be fairly complex since there is no restriction on the densities except for the conditions that all PDFs must adhere to. For theoretical consistency, all PDF's should be non-negative and integrable everywhere and their integral over the whole domain should equal one. A similar decision rule has been established for many category problems (Specht 1967).

In cases when the a priori probabilities are equal to each other and the loss function are assumed to be the same, Bayes rule classifies an input pattern to the class that has its PDF greater than the PDF of the other class for that input pattern. Hence, the effectiveness of this procedure depends on the accuracy of the PDF estimation. Hence, the first step is the computation of the PDF's $f_A(X)$ and $f_B(X)$ in order to compute the decision boundary. The PDF's can be computed using a Parzen window considering a multivariate kernel as shown in (6). The procedure of construction of a family of estimates of the PDF, $f(X)$ was shown by Parzen and Cacoullos (Cacoullos 1966). It extended Parzen's results to the case where a multivariate kernel is a product of univariate kernels. When a Gaussian kernel is used, the multivariate estimate for PDF can be expressed as

$$f_A(X) = \frac{1}{(2\pi)^{p/2}\sigma^p}\frac{1}{m} \times \sum_{i=1}^{m} \exp\left[-\frac{(X - X_{Ai})^T (X - X_{Ai})}{2\sigma^2}\right] \tag{6}$$

where X is the vector to be classified, $f_A(X)$ is the value of the PDF of category A at point X, m denotes the number of training vectors in category A, p is the dimensionality of the training vectors, X_{Ai} is the ith training vector for category A, and σ is the smoothing parameter. $f_A(X)$ can be determined by summing the multivariate Gaussian distributions centered at each training sample. However, the sum is not limited to being Gaussian.

Figure 1 shows a well-known architecture of a PNN for classifying the vector X into two categories A and B. It consists of four different layers, including the input layer, pattern layer, summation layer and the output layer. The input units are merely distribution units that provide the same input values to all the pattern units. Each pattern unit

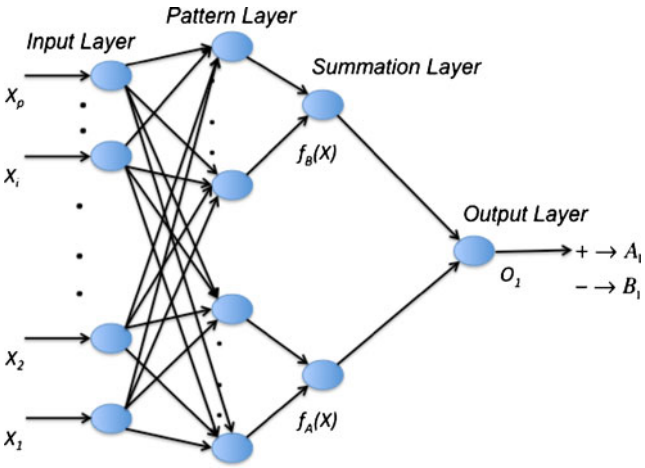

Fig. 1 Architecture of probabilistic neural network

forms a dot product of the input pattern vector X with a weight vector W_i, such that $Z_i = X.W_i$. After this operation Z_i is passed through a nonlinear operation which is then summed together to form the PDF using the Parzen window in the summation layer. For an exponential nonlinear operation the PDF can be calculated by summing the exponential functions as shown in (6).

In Fig. 1, the second layer of the PNN architecture is the pattern layer which can be interpreted as Fig. 2a. In the pattern layer, the first step of training the network is to set the weight vector W_i in one of the pattern units equal to each of the X patterns in the training set. In fact, W_i's are the class indices of the corresponding X_i. Each pattern unit then forms a dot product of the input pattern vector X with the weight vector W_i—namely, $Z_i = X \cdot W_i$. Then, the nonlinear operation depicted in (6) can be performed on Z before passing the output of this step to the summation unit (Fig. 2b).

In contrast to the sigmoid transfer function (Hornik et al. 1989) that is generally used for backpropagation networks, the transfer function used in this PNN is the exponential function—namely, $g(Z_i) = exp[(Z_i - 1)/\sigma^2]$. If both X and W_i are normalized to unit length, the nonlinear transfer function can be expressed as,

$$g\left(Z_i\right) = \exp\left[-\frac{\left(W_i - X\right)^T \left(W_i - X\right)}{2\sigma^2}\right] \tag{7}$$

Once the transfer function has been calculated, the outputs corresponding to class A and B can be summed together in the summation layer to compute the PDF using the Parzen window method according to (6).

Figure 2b represents the summation layer which is used to calculate the class or category PDFs from (6). This step involves connecting the pattern unit's output to the appropriate summation unit. Every training pattern requires a separate neuron (pattern unit). The same pattern units can be grouped by different summation units to provide additional pairs of categories and additional bits of information in the output vector. This is illustrated in Fig. 1 for the case where all the pattern layers are grouped into two categories for the classification of X into either of the two classes A or B. Furthermore, once the class PDF's $f_A(X)$ and $f_B(X)$ are computed, the Baye's decision criteria can be evaluated by the following equations,

$$d\left(x\right) = \theta_A \quad \text{if} \quad f_A\left(x\right) + C_k f_B\left(X\right) > 0 \tag{8}$$

$$d\left(x\right) = \theta_B \quad \text{if} \quad f_A\left(x\right) + C_k f_B\left(X\right) < 0 \tag{9}$$

$$\text{and } C_k = -\frac{h_{B_k} l_{B_K}}{h_{A_k} l_{A_K}} \cdot \frac{n_{A_k}}{n_{B_k}} \tag{10}$$

where n_{A_k} and n_{B_k} are the number of training patterns from category A_k, and the number of training patterns from category B_k, respectively.

It can be seen from (8) that C_k is the ratio of a priori probabilities divided by the ratio of samples multiplied by the ratio of losses. Thus, if the number of training samples from categories A and B are in proportion to their a priori probabilities, then $C_k = -l_{B_k}/l_{A_k}$. The final ratio, C_k, cannot be calculated from the statistics of the training samples

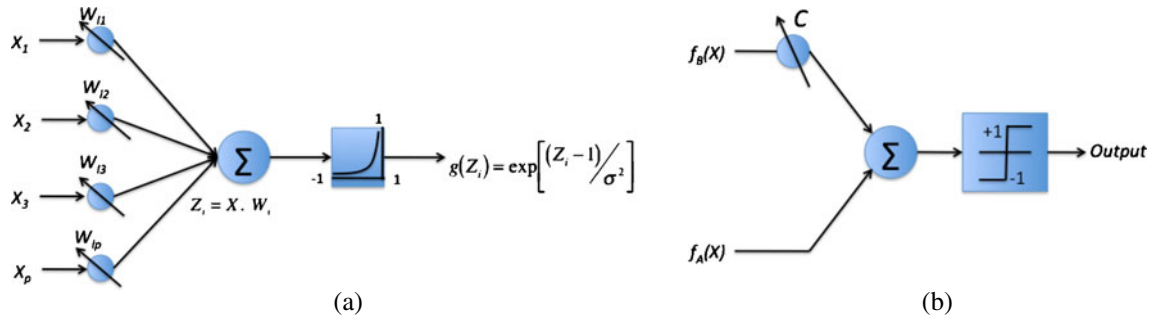

Fig. 2 Architecture of second and third layers for PNN. (**a**) Pattern layer (**b**) Summation layer

alone, but only by the significance of the decision. If there are no strong reasons for biasing the decision, then C_k can be simplified to -1. In all the representative examples in this paper, C_k has been taken as -1.

By adapting the classification procedure, the PNN can be used for the estimation of the reliability constraints in the RBTO problems. In the reliability estimation process, the input training vector X is a data point generated using random sampling methods, such as Monte Carlo sampling (MCS) or Latin Hypercube sampling (LHS) (McKay et al. 1979). Once the PNN network is trained and the PDF's $f_A(X)$ and $f_B(X)$ are generated, the test data can be classified by evaluating the Bayes decision function in (8) and (9). By evaluating the number of points in each class, the probability of failure (P_f) value can be calculated for the topology optimization procedure. More details of this aspect will be discussed in the following sections.

3 Topology optimization under uncertainty

The main objective of the topology optimization is to fulfill the objective function with the minimum amount of material layout possible. Less amount of material usage leads to reduced cost of the overall structure, and the less number of parts in the final structure makes the final structure easier to assemble. A concept of reliability analysis can be incorporated into the deterministic topology optimization method; this incorporated scheme is referred to as Reliability-based Topology Optimization (RBTO). In RBTO, the statistical nature of constraints and design problems are defined in the objective function and probabilistic constraint. The probabilistic constraint can specify the required reliability level of the system. The formation of RBTO is similar to that of deterministic optimization:

$$\textbf{\textit{Min/Max:}} \quad f\,(b)$$

$$\textbf{\textit{Subject to:}} \quad P_j\left[g_j\left(b, \underline{x}\right) < 0\right] \leq P_{Rj} \tag{11}$$

$$\sum_{i=1}^{N} A_i L_i - V** \leq 0 \tag{12}$$

$$b_l \leq b \leq b_u \tag{13}$$

$$Ku = F \tag{14}$$

where $f(.)$ represents the objective function, $g_j(.)$ represents the limit-state function, b is the vector of deterministic design variables, and $\underline{x}$ is the random vector, which can be random design variables or random parameters of the system. In (11), $P_j[\cdot]$ denotes the probability of the event, and the probability of failure, P_f, can be defined as $P_j[g_j(\cdot) < 0]$. is the specified probability of failure (P_f) level. A_i is the cross-sectional area of the elements and L_i is the length of that particular element. $V*$ denotes the volume of material that can be used in the final design. A_l and A_u are the upper and lower bounds on the cross-sectional area of the elements, respectively. K is the global stiffness matrix, u is the global nodal displacement vector and F is the nodal load vector.

Most of the time, $V*$ is given as a fraction of the maximum possible volume of the structure, i.e., in the case where all the design variables go to their upper bound, A_u. Hence, (12) represents the volume constraint. Within every iteration in the optimization processes, the finite element analysis (14) is invoked and the information required by the objective function is evaluated. Due to the nature of the reliability constraint (11) in the RBTO problem, it is critical to consider realistic uncertainty representation schemes to conduct accurate reliability assessment. In the current research, the random field (Choi et al. 2006) representation is considered to model input uncertainties. A random field is a random function of one or more variables. Many distributed properties in structural systems are random. Efficient and realistic representation of the inputs will facilitate accurate estimations of random responses' statistics. However, traditional deterministic analysis, such as the finite element method, uses a single design point, considering it sufficient to represent the response. This simulation of a single design point is inadequate and unrealistic when characterizing systems under varying loads and material properties. For instance, in studying the response of an aircraft to gust loads, we cannot cover all types of gusts and speeds in a single simulation. The mathematical model of the spatial variability, parameterized by the correlation between different locations, can be characterized by means of a random field. The basic idea of the random process is that the outcome of each experiment is a function over an interval of the domain rather than a single value. Thus, analysis of the random process is a realistic approach that can produce a whole design space instead of just a one-point result. The resulting function, which is generated for all the points as inputs (x_1,..., x_n) in the sample space Ω, is known as a realization of a random process, and the collection of realizations is referred to as an ensemble (Choi et al. 2006). When a set of samples in the interval, $[t_0 t_n]$, is considered, the joint probability distributions of n random variables U can specify the particular random process (Fig. 3). Thus, the moments of the random process $U(t)$ can be defined by similar formulas in accordance with the definition of the moments of the random variable. The PDF of the random process $U(t)$ can be specified as $f_U(u, t)$. In particular, if the PDF is independent of t, namely $f_U(u, t) = f_U(u)$, then the process is referred to as a stationary process; otherwise it is called a

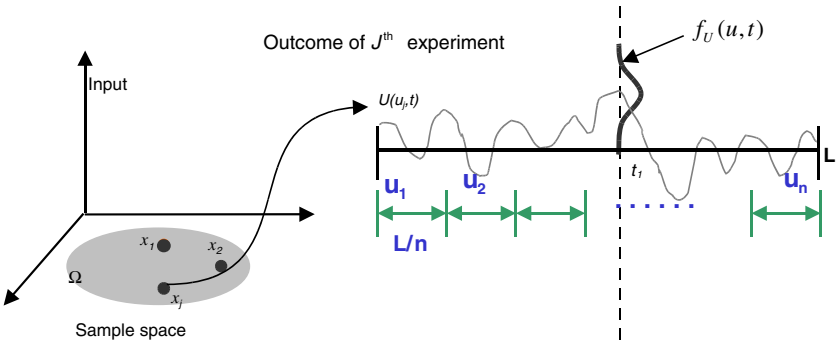

Fig. 3 Illustration of a random process

non-stationary process. Accordingly, all the moments of the stationary process are independent of$t$ in this case.

A cantilever beam of length L, which is discretized into n sections, is represented by the discretized random field as shown in Fig. 3. Here $(u_1, u_2, ..., u_n)$ represent properties of the beam that vary along the length of the cantilever beam and $(x_1,..., x_n)$ represent the samples which are generated during the Jth experiment. In this paper the random variables $(x_1,..., x_n)$ are generated using MCS/LHS and Young's modulus of elasticity E is considered as the property that varies along the length of the structure. This random field discretization can be used to describe the spatial variability of the stochastic structural properties over the structure. In this discretization procedure, the particular value of E_n is assumed to have the same value for the entire nth segment and its accuracy depends on the size of the segments. After this discretization procedure, the random field can be replaced by a set of correlated random variables.

The discretization of the random field is similar to the finite element discretization of structures. In the discretization procedure, the particular value of U_n is assumed to have the same value for the entire nth segment, and its accuracy depends on the size of the segments. After the discretization procedure, the random field can be replaced by a set of correlated random variables. Several methods have been suggested to produce the random field representation. In the current research, the Karhunen-Loève expansion (Hotelling 1933; Chien and Fu 1967; Fukunaga and Koontz 1970) is considered, which utilizes the collections of eigenfunctions and eigenvalues to represent random fields.

In the Karhunen-Love expansion, the series of the eigenfunctions and the eigenvalues form the random process:

$$u(x) = \sum_{i=1}^{\infty} \sqrt{\lambda_i}\xi_i\phi_i(x) \tag{15}$$

where ξ_i is a set of uncorrelated random variables, and this expansion expresses the projection of the random process $u(x)$. The eigenfunctions, $\phi_i(x)$, and eigenvalues, λ_i, can be estimated from

$$\lambda_i\phi_i(x) = \int S(x, y)\phi_i(y)dy \tag{16}$$

where $S(x, y)$ is the covariance function, and x and y are the temporal or spatial coordinates.

In the discrete case, (16) can be specified by a statistical interpretation of the eigenvalue problem

$$[P][\Lambda] = [S][P] \tag{17}$$

where the covariance matrix $[S]$ is a symmetric and non-negative definite matrix, and $[P]$ and $[\Lambda]$ are the orthogonal eigenvector matrix and the eigenvalue matrix, respectively.

Consequently, the orthogonal decomposition of the covariance matrix provides the product of the matrices of eigenvectors and eigenvalues

$$[S] = [P][\Lambda][P]^T$$

$$\text{or } [S] = [A][A]^T \tag{18}$$

where $[A]$ is the transform matrix chosen as $[A] = [P][\Lambda]^{1/2}$.

The transform matrix $[A]$ can be employed to yield the correlated random vector T:

$$[T] = [A][U] \tag{19}$$

where $[U]$ is the $n \times 1$ matrix of uncorrelated random variables U_j, $(j = 1,...,n)$, and the transformed matrix, $[T]$, possesses a given covariance matrix $[S]$.

4 Proposed framework using PNN

Figure 4 illustrates the framework for topology optimization using a classification process based on PNN. The overall framework consists of two blocks. The left block is the block where the topology optimization procedure is conducted and the right block is responsible for conducting the reliability analysis using the PNN procedure. In the beginning of the procedure the designer has to input the force and boundary conditions on the initial layout structure (ground-truss). A limit state function $g(x_i)$ depicts the failure property of the structure. For many practical applications the limit state functions can be set as a limit on

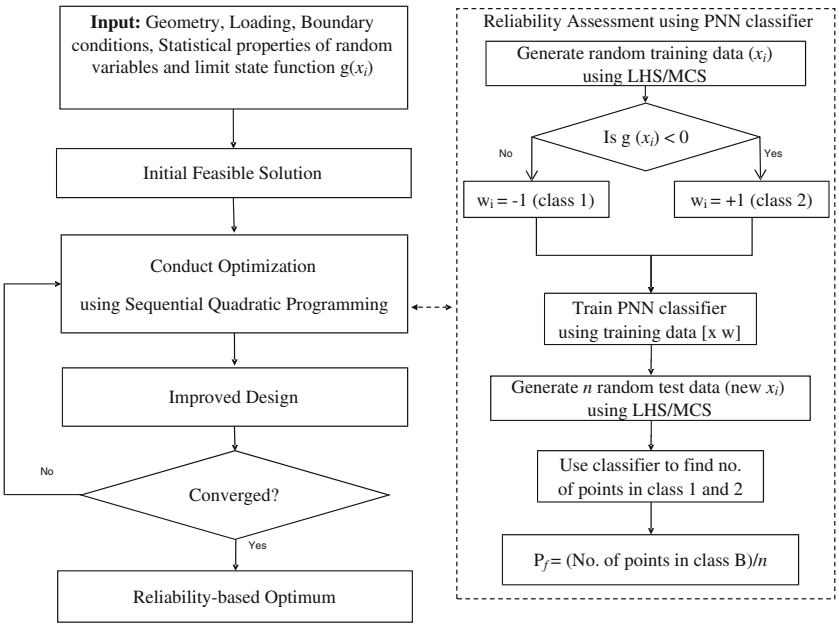

Fig. 4 Proposed framework using PNN

the displacement of a node on the ground-truss. A volume fraction is specified which is a fraction of the desired final volume of the structure and the maximum possible volume of the structure if all the truss elements exist at the upper bound of area of cross-sections. A finite element analysis procedure is used to evaluate the limit state function and the objective function. Sequential quadratic programming is used for the optimization procedure. In order to evaluate the reliability constraint (10) the right block of the framework in Fig. 4 is invoked. The evaluation of the reliability constraint requires the evaluation of key parameters using FEM, which is computationally expensive. Hence the classification procedure using PNN is used to reduce the computational requirement of the overall procedure. Using PNN as a surrogate model reduces the number of times FEM procedure is invoked, resulting in a drastic reduction of computational requirement.

The reliability estimation procedure consists of two steps. The first step in this procedure is the generation of training data for which $g(x_i)$ is evaluated. The random variable x_i can be generated from a given PDF using LHS. For most of the cases a normal distribution assumption is sufficient to insert uncertainty into the optimization process. Hence, for this paper all the data generated was from a normal distribution. The estimation in this case is a class w which is assigned a value of -1 if the structure is safe and a value of $+1$ if the structure is in the failure region for the generated x_i values. The points having a value of -1 for w can be considered to be from class A and those with value of $+1$ can be considered to be from class B. Once the w_i's are obtained for all x_i's, the training data is prepared having a form of $[x\,w]$. This data is then used to train the PNN classifier. Figure 4 illustrates this procedure for the case where n random variables (x_i) are generated using LHS and the estimate w is computed for each of the new samples.

This data is used to train the PNN classifier. Hence, a new classifier is trained during every iteration of the optimization algorithm. After training, the second step in reliability estimation is the generation of test data. Test data is generated using LHS which is classified by the trained PNN classifier into either of the two classes. The probability of failure is then calculated in the last step using (20).

$$P_f = \frac{\text{No. of points in class B}}{n} \tag{20}$$

The P_f value is then passed to the optimization algorithm where the convergence of the solution is checked. The optimization algorithm stops when the solution converges to a reliable solution.

4.1 Disjoint failure region example

In this example, the applicability and usefulness of the PNN for the disjoint failure problem will be demonstrated with an analytical problem. Consider a limit state function with two random variables,

$$g(u_1, u_2) = u_2 - |\tan(u_1)| - 1 \tag{21}$$

where u_1 and u_2 are assumed to be Gaussian random variables.

This example consists of two phases, namely the training phase and the test phase. During the training phase of the PNN, 500 samples of u_1 and u_2 are generated using LHS with an assumption of Gaussian distribution $\sim N(4, 16)$. Accordingly, the structure is considered to be safe if

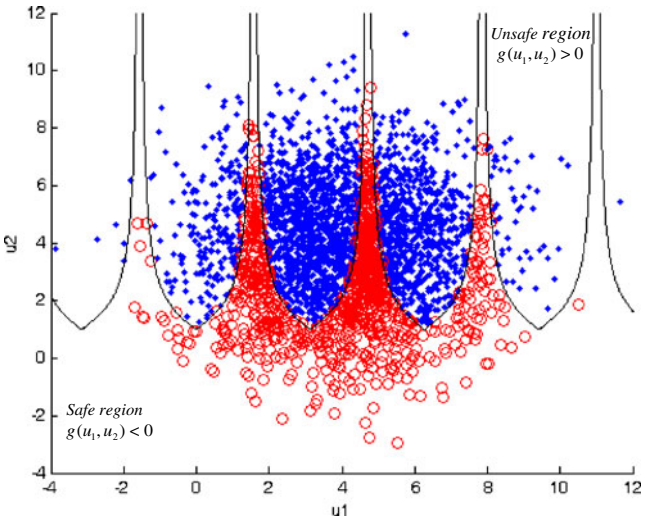

Fig. 5 Data points classified into safe and unsafe regions

$g(u_1, u_2) < 0$ and the structure is considered to have failed if $g(u_1, u_2) > 0$. The points in the safe region can be given a class label of $w_i = -1$ (class A) and the points in the unsafe region can be given a class label of $w_i = +1$ (class B). Depending on the sign of $g(u_1, u_2)$, each data point is assigned a class w_i. Once the PNN was trained, 3,000 data points were generated using LHS in order to test the classifier. This comprises the second phase of this example where the P_f is calculated using the PNN.

The PNN was applied to classify the data points depending on whether they fall into the failure region or the safe region. In this procedure, the *radial basis* neurons (Hornik 1991) are utilized for which weighted inputs are calculated using the Euclidean distance of the data point from the origin. The exponential nonlinear transfer function (6) used in the pattern layer with the smoothening parameter or spread, σ value of 0.3. After using the exponential function in the pattern layer of the PNN, the response is passed to the summation layer where the PDF's are calculated and summed together to obtain the decision boundary, which was depicted in (8) and (9). The loss functions and the a priori probabilities are assumed to be the same for both classes which results in

$$C_k = -\frac{n_A}{n_B} \tag{22}$$

The safe and unsafe regions for the given problem are shown in Fig. 5. The function of the limit state function, $g(u_1, u_2)$, is plotted as solid line in Fig. 5. As mentioned earlier, 500 points were sampled using LHS for training the PNN classifier and 3,000 points were sampled for evaluating the probability of failure. The points from the test data that are in the safe region are represented by circles and the points in the unsafe region are represented by dots in Fig. 5. In order to validate the efficacy of the proposed method, MCS is conducted with 10,000 samples to evaluate the probability of failure. The results obtained from this example are summarized in Table 1. The P_f value calculated using the classification procedure is different from the MCS value by 1.67% which was concluded to be well within the acceptable threshold for reliability estimation. The result Table 1 confirms that classification procedure provides sufficient accuracy compared to the results from MCS in this disjoint failure domain problem.

Hence a PNN based classification procedure is highly effective in the case of disjoint failure domain problems. A PNN based reliability estimation procedure can be used by a designer in order to preempt the case of disjoint failure domain problems in most cases, where the designer is unaware of the failure behavior of the system beforehand. The following section will demonstrate the applicability of the PNN procedure to the framework of the RBTO problem.

4.2 Stiffest structure design via classifcation-based RBTO under random fields

The stiffest structure problem in topology optimization, namely the minimization of compliance (maximization of stiffness) for a given total mass of the structure, is considered to show the efficacy and applicability of the developed framework. In this section, two example problems are considered to demonstrate the effectiveness of the current framework when buckling loads are employed. In the first case, the deterministic solution will be compared to a stochastic solution obtained while considering a displacement limit state function. In the second case, the RBTO problem will be solved while considering a buckling limit state function. The stochastic solution obtained using the buckling limit state function will be compared to the other solutions to show the efficacy of the proposed framework with respect to disjoint failure domains in the topology optimization problem.

The objective function of the first case is considered to be the minimization of strain energy for the structure when

Table 1 Results from the disjoint failure domain example

	Classification (3,000 samples)	MCS (10,000 samples)	Difference (%)
P_f	0.6890	0.7007	1.67

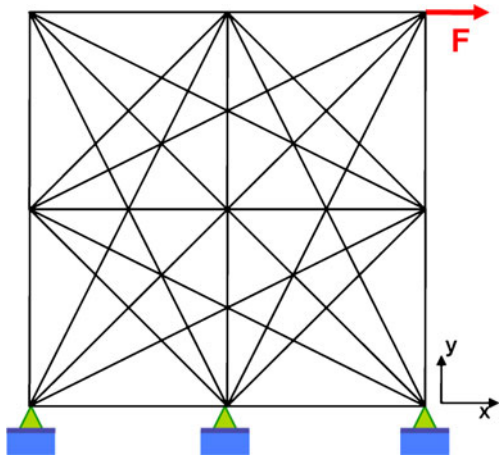

Fig. 6 Representation of ground truss problem for solving the stiffest structure problem

the cross-sectional areas are the design variables. A volume constraint specifies the maximum amount of material that can be used for the layout of the truss structure. The optimization statement for the ground structure example is represented as

$$\begin{aligned} &\textbf{\textit{Minimize:}} \quad \text{Strain Energy} \\ &\textbf{\textit{Subject to:}} \quad P_j[g_j(b, \underline{x}) < 0] \leq 0.0001 \end{aligned} \tag{23}$$

$$\sum_{i=1}^{N} A_i L_i - V** \leq 0 \tag{24}$$

$$A_l \leq A \leq A_u \tag{25}$$

$$Ku = F \tag{26}$$

where b represents the deterministic design variables A_i and x represents the uncertain parameter in the RBTO process. For this problem the uncertain parameter introduced in the problem is the Young's modulus, E.

The 3×3 ground truss example is shown in Fig. 6. The ground truss structure contains nine nodes in total and all nodes are interconnected with truss elements with the help of pin joints. All the elements in the ground truss are assumed to be either in tension or compression only. Bending and buckling effects are assumed to be negligible. The number of truss elements is 28. The boundary conditions of the nodes of the bottom part are fixed and a force of 100 N is applied at the top-right node. The length of each side of the square shaped ground structure is 100 mm and the Young's modulus of the structure is assumed to be 2.1×10^5 N/mm^2 with a Poisson's ratio of 0.3. The upper bound on the cross-sectional area is taken as 10 mm^2 and the lower bound is taken as 10^{-4} mm^2. A volume fraction of 0.3 is taken for the volume constraint, which constrains the desired volume of material used in the final structure to be 30% of the maximum possible volume, if all the truss elements had their areas of cross-sections at their upper limit.

Ideally the designer would like the design variables to converge to either the lower bound or the upper bound. However, intermediate values of the design variables are seen many times. Hence it is advisable to create intermediate values where the design variables can converge. The designer should consider intermediate values according to the manufacturing constraints or other designer's preference. In this paper the intermediate values of 3 mm^2 and 7 mm^2 are chosen. Figure 7 shows the optimum truss structure for the deterministic case, which does not include the reliability constraint as shown in (23). Five truss elements are remaining in the final solution as shown in Fig. 7a. All the truss elements have a cross-sectional area of 10 mm^2. The rest of the truss elements converged to the lower bound and none of the elements had the intermediate values of 3 mm^2 and 7 mm^2. This optimization problem was solved using a traditional optimization algorithm, i.e., the Sequential Quadratic Programming (SQP) method. As the number of elements are increased corresponding to the increase in the number of nodes in the x- and y-axes, the time taken

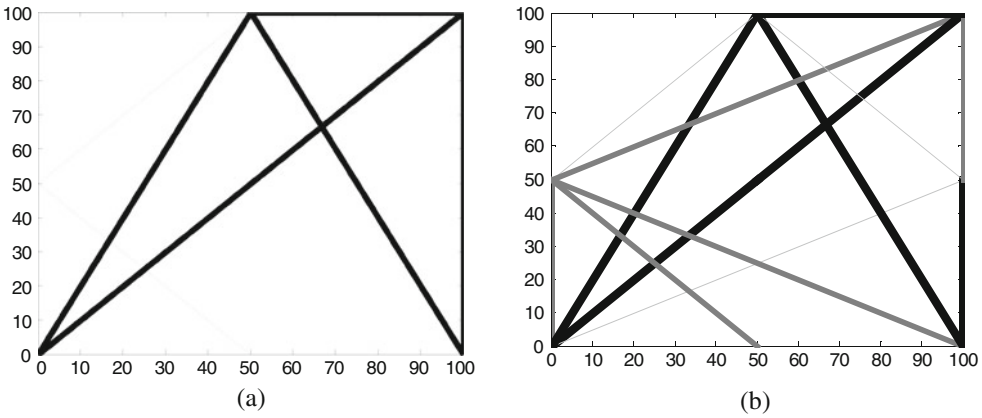

Fig. 7 Optimization solution for ground-truss. (**a**) Deterministic optimum (**b**) Stochastic optimum

for convergence increases at a much faster rate. This structure does not guarantee to resist failure in the wake of uncertain boundary conditions and material properties. For a truss structure to resemble a material design, the material structure should be able to endure various boundary conditions.

For the stochastic optimization case, all the given conditions are the same as the deterministic problem except for the consideration of the reliability constraint (23). Young's modulus, E, of each element is considered as a random variable ($\mu_E = 2.1 \times 10^5$ N/mm^2, COV $= 0.1$). These uncertain parameters are assumed to vary according to a random field corresponding to the random function U in Fig. 3. Figure 8a illustrates the Gaussian covariance model ($C_{ij} = \sigma^2 exp(-(x_{ij}/l)^2)$ assumed to have a correlation length, l, of 50. Figure 8b clearly shows different levels of Young's modulus using color scales for one realization.

To consider the constraint of the probability of failure, the limit state function is taken as the displacement, u, in the positive x-direction at the top-right node; namely, $g(u) \leq 0.01$. The probability of failure level is chosen as $P_f = 10^{-4}$ in (23). 100 samples were generated using LHS which would represent variable material property for the truss structure. These variable Young's modulus values represent the input variable x from Fig. 3. The displacement at the top-right end node is calculated using the FEA for the 100 cases. In order to estimate the system response for subsequent cases, a PNN was trained using radial basis functions in the pattern layer.

After completing the training of the PNN, P_f was calculated with the trained PNN based on the number of displacement values that exceed the limit state function, $g(u)$, using MCS with 10,000 samples. Again, the optimization problem was solved using SQP method, and the corresponding stochastic optimum is shown in Fig. 7b. The stochastic procedure distributed material in a wider space and contains more truss elements than the deterministic procedure. While the solution obtained from the stochastic procedure has 13 elements, the one obtained using the deterministic optimization procedure contains 5 significant elements.

Of the 13 elements, 5 elements are the darkest which signifies that they have an area of cross-section area of 10 mm^2. The 3 elements which are the thinnest have an area of cross-section of 3 mm^2 and rest of the elements have an area of cross-section of 7 mm^2. Specifically, the volume of the stochastic structures is 6.18×10^3 mm^3.

Incorporating a buckling constraint as the limit state function will enable the design of structures which are resistant to buckling. Since buckling is a disjoint failure criteria, classification based architecture will be more appropriate as a surrogate modeling technique than a regression based approach.

The limit state function in this case is expressed as buckling failure criteria where the structure will be marked as failed if the stress due to compression in any truss member exceeds the Euler buckling stress. Euler buckling stress for a truss member with circular cross-section can be expressed as:

$$\sigma_{icr} = -\frac{\pi E A_i}{4L_i^2} \tag{27}$$

The limit state function can then be expressed as

$$g(P_i) = \sigma_{icr} - \frac{P_i}{A_i} \tag{28}$$

where P_i represents the reaction force in each truss member. The reaction forces are calculated using the FEA during every iteration of the optimization algorithm. The limit state function is only considered for the truss members in compression since buckling is a compression stress phenomenon. The limit state function in (28) gives a negative

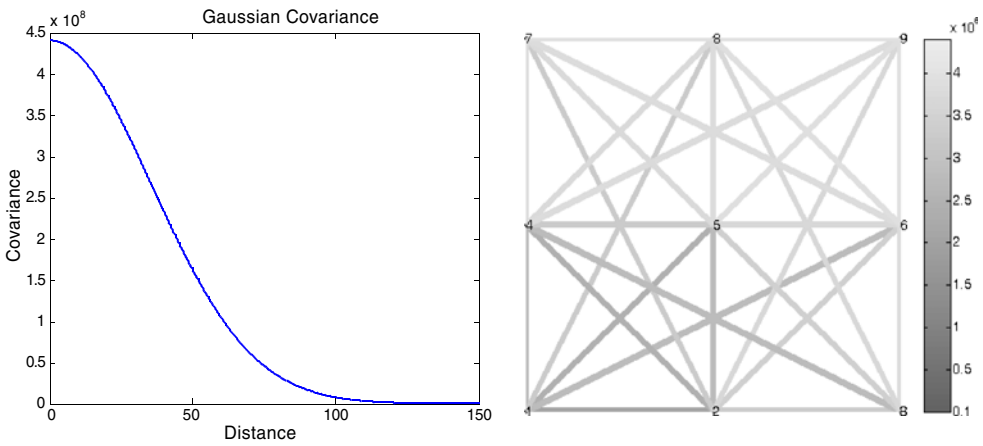

(a) (b)

Fig. 8 Uncertain properties of stiffest structure problem. (**a**) Gaussian covariance model ($l = 50$ mm) (**b**) Random field realization of elastic modulus

value in case any of the truss elements in the structure buckles. The Young's modulus is considered as the random variable which is assumed to vary as a random field in a similar fashion as in Fig. 8. The optimization problem was solved using the sequential quadratic programming algorithm and the solution is shown in Fig. 9. Compared to the stochastic solution shown in Fig. 7b, the buckling constraint based solution doesn't contain any members with 3 mm^2 area of cross-section. The total number of truss elements in this truss structure is 10 compared to 13 in the stochastic solution of Fig. 7b. A clear change in the material distribution can also be seen. In general the number of elements in the stochastic solution is larger than that obtained for a deterministic solution. Similar result has also been observed by Seepersad et al. in 2006. In order to validate the reliability of the structure, the P_f value of the three structures shown in Figs. 7 and 9 were evaluated using 20,000 samples generated using MCS. The obtained stochastic solution (Fig. 9) with buckling limit state function has a P_f value of 0.56×10^{-4} which represents a 70.37% decrease in P_f value from the deterministic solution's (Fig. 7a) P_f value of 1.89×10^{-4}. Furthermore the P_f value of the solution in Fig. 9 achieves a P_f value which is 27.27% lower than the P_f value for the stochastic solution in Fig. 7b. The obtained result demonstrates the superiority of the proposed method compared to the traditional deterministic procedure in the presence of random fields.

4.3 Stiffest structure design for a hydrogen storage tank

One of the most technically difficult tasks impeding widespread use of hydrogen as an energy source is developing safe, reliable, compact, and cost-effective methods for storing hydrogen. This is a challenging task due to the significant amount of space required to store enough quantities of hydrogen. For light-duty vehicular applications the available compressed hydrogen tanks are larger and heavier than necessary. A possible solution to the above mentioned problems is the design of a storage tank utilizing mesostructures as the inner lining of a rigid hydrogen storage tank. Using a mesostructure inner lining will help in reducing the weight of the overall structure. In the synthesis of truss-based mesostructures, a 2D structure can be offset and connected to form the desired mesostructure. Hence after the transformation, the 3D structure manufactured might not have the same properties that it was designed for in 2D. Design of a hydrogen storage tank using 2D ground-truss was explored in Patel and Choi (2009). The following example illustrates the procedure of designing a reliable mesostructure inner lining of a rigid hydrogen tank using the proposed RBTO procedure. Once the 3D mesostructure is designed, it can be copied along the body of the hydrogen tank for improved performance over preexisting mesostructure-based inner linings.

The 3D ground-truss can be assembled together to form the inner lining as shown in Fig. 10. It is important to note that this procedure of assembling unit cells to produce the final structure is motivated by the fact that assembling similar unit cells together will be less computationally expensive in the design process. Making a structure with similar kinds of unit cells will also reduce the manufacturing effort drastically. Hence this example illustrates a method of design of a thin walled pressure vessel where the solid thin wall is replaced by identical unit cells. The stress on a thin walled pressure vessel with the geometry described above is broken up into the hoop stress, σ_h and radial stress σ_r which are determined as follows

$$\sigma_h = \frac{\mathrm{Pr}}{t} \tag{29}$$

$$\sigma_r = \frac{\mathrm{Pr}}{2t} \tag{30}$$

where P, r and t are pressure, inner radius and thickness of the tank, respectively. It is important to note that (29) and (30) are derived for a thin walled pressure vessel. For

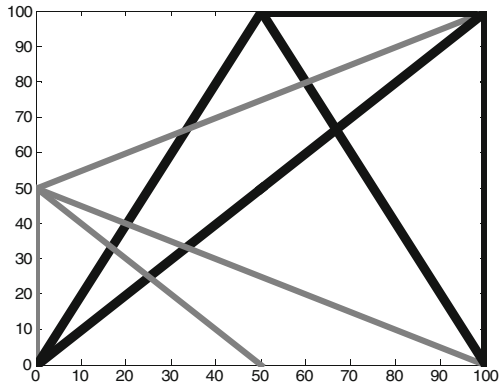

Fig. 9 Design solution with buckling limit state function

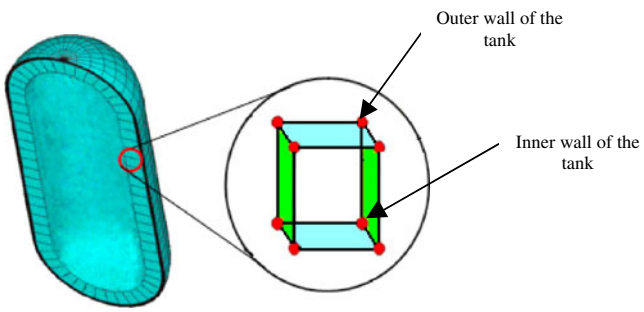

Fig. 10 Discretization of hydrogen tank into 3D groundtruss structures

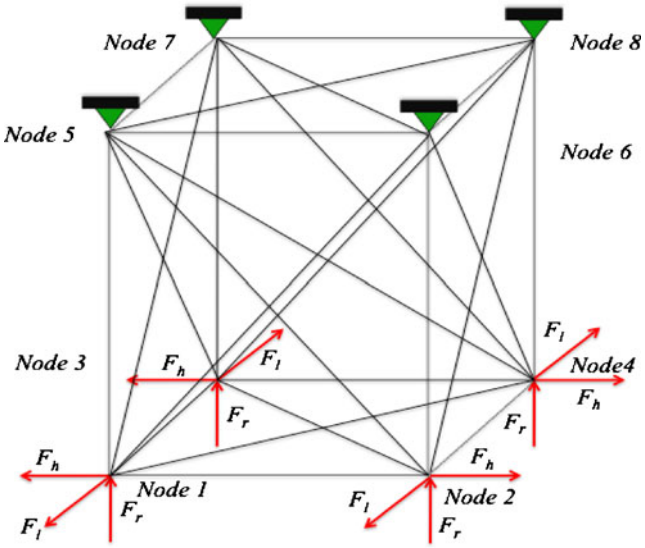

Fig. 11 Representation of the groundtruss problem in 3D

simplicity, the authors assume that (29) and (30) are valid for the case where walls of the pressure vessel are thin and consist of internal truss structures. Since the solid material within the walls of the hydrogen storage tank is replaced by internal truss structures, the forces that will be calculated by using (29) and (30) will be assumed to be the same for the case when the walls of the hydrogen storage tank is composed of internal truss structure. The internal truss structure will be designed using the proposed RBTO procedure where each of the internal truss elements will be reliable against buckling.

The given storage tank used for the RBTO procedure has a length of 1.35 m and an inner radius for the cylindrical portion of the tank of 0.3 m. The wall thickness is given as 8.29 mm. The internal pressure of the tank is given as 25.4 MPa. The storage tank is assumed to be made of steel alloy with a Young's Modulus of 379 GPa and a Poisson's Ratio of 0.2. According to the information gained from the solid wall analysis, the chosen size of the unit cell is a square with dimensions equal to that of the thickness of the tank which is 8.29 mm. From the given internal pressure, the hoop stress and radial stress are calculated using (27) and (28). Since the devised RBTO algorithm only accepts forces acting at nodes, these stresses are converted to point loads acting at the bottom nodes of the unit cell. The values of the forces due to these stresses are $F_h = 67{,}818$ N, $F_r = 33{,}909$ N and $F_l = 2{,}012$ N. In order to obtain the stiffest structure for the hydrogen storage tank inner lining problem, the minimization of strain energy is considered as the objective function. The corresponding RBTO optimization statements are also represented by (23)–(26). In this case x in (23) represents the Young's modulus of the truss elements which are considered as random variables in this example. The uncertainty is assumed to be only in the material properties. Hence a Gaussian variation is assumed for the Young's modulus of each truss element.

Figure 11 shows the force and boundary conditions on a 3D ground-truss structure. There are 8 nodes in this structure, and each node is connected with every other node using truss elements. Nodes 5, 6, 7 and 8 are grounded suppressing all displacement degrees of freedom for these nodes. In grounding nodes 5, 6, 7 and 8 we have assumed that the outer layer of the hydrogen storage tank is not allowed to expand or contract; whereas, the total number of truss elements in this groundtruss is 28. The length of each side of the square shaped ground structure is taken as 8.29 mm for simplicity since the thickness of the hydrogen tank also corresponds to 8.29 mm. The smoothening parameter, σ, is set to 0.3 for the PNN procedure. A set of 300 training data was generated to train the PNN classifier. Once a classifier model was constructed using the PNN, LHS with 2,000 sampling points was applied to evaluate the reliability constraint. The obtained solution of the RBTO problem is depicted in Fig. 12b. The deterministic topology optimization solution is shown in Fig. 12a. Both the deterministic solution and the stochastic solution have 14 elements in the final solution. The deterministic solution is composed of truss elements having a cross-sectional area of

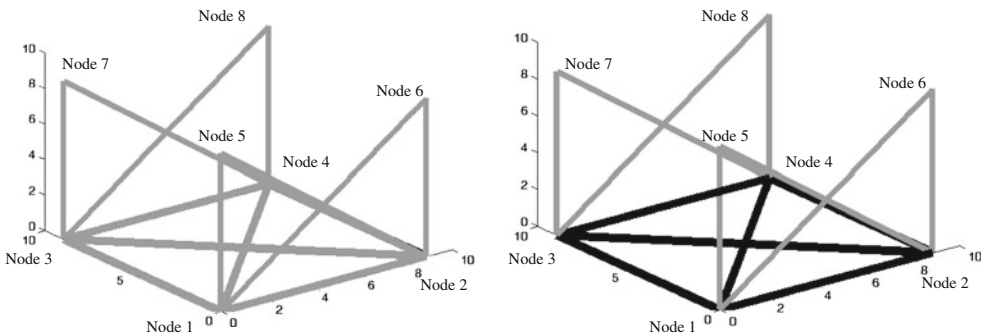

Fig. 12 Stochastic optimum using the RBTO with the PNN. (**a**) Deterministic optimum (**b**) Stochastic optimum using PNN

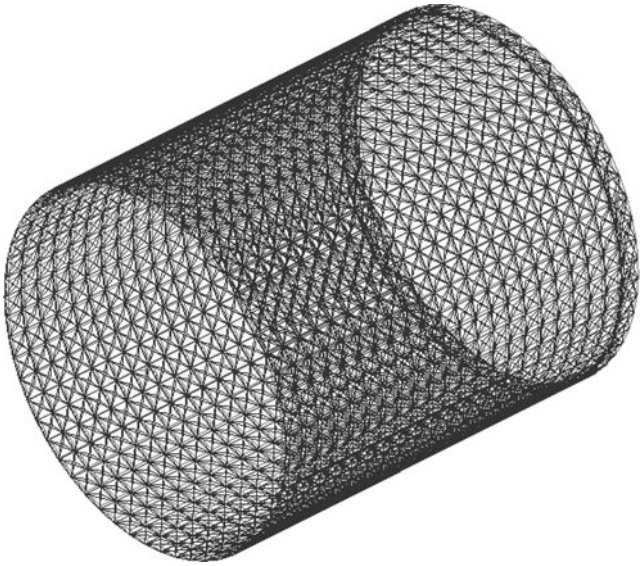

Fig. 13 Mesostructured cylindrical surface of tank

7 mm^2 whereas the stochastic optimum has truss elements consisting of cross-sectional areas of 7 mm^2 and 10 mm^2. The inner layer of the hydrogen storage tank consists of nodes 1, 2, 3 and 4 which are depicted in Fig. 12b to be joined by black colored truss members. The black truss members represent members with a 10 mm^2 area of cross-section. The final volume corresponding to a volume fraction of 0.3 of the reliability-based optimum solution is 1.077×10^4 mm^3.

The solution obtained in Fig. 12b can be copied around the cylindrical section of the inner surface of the tank to obtain the mesostructured inner lining of the hydrogen storage tank. Nodes 1, 2, 3 and 4 constitute the inner surface of the inner lining; whereas, nodes 5, 6, 7 and 8 constitute the outer surface of the lining which will be in contact with the rigid wall of the tank. Since a fixed boundary condition was applied on nodes 5, 6, 7 and 8, it can be assumed that the expansion and contraction of the tank in the lateral direction is negligible. According to this modeling simplification the designer can put a skin on top of nodes 5, 6, 7 and 8. Figure 13 shows the cylindrical surface of the hydrogen storage tank which has a skin on the top surface. Since there is a uniform pressure distribution inside the hydrogen storage tank, the mesostructure designed in Fig. 13 is a reliable solution to the hydrogen storage tank inner lining in all locations. Note that this assumption of uniform pressure enables us to assume that all the unit cells in the inner lining will be exposed to the same boundary conditions. To simplify the computational costs in the optimization process, it is also assumed that the uncertainty in material properties varies for all truss elements together to avoid varying the Young's modulus for each truss element independently. Thus, the same unit cell will satisfy the requirements at all locations of the inner lining. However, this assumption is not the limitation from the proposed method. It is also possible to consider all the truss elements in the whole inner lining structure during the proposed design process. With the final design of Figs. 12b and 13, the probability of failure of the overall structure was determined to be 9×10^{-5} when the P_f value for the structure was calculated using 1,000,000 samples of LHS.

There is an alternative way of designing the inner lining structure. It is possible to include the inner and outer skins as permanent truss elements in the optimization of ground truss. In this case, the groundtruss represented in Fig. 11 will have permanent truss members between nodes 1, 2, 3 and 4, which constitute the inner surface and between nodes 5, 6, 7 and 8, which constitute the outer surface. Figure 14 shows the optimal designs of deterministic and stochastic cases by considering the permanent truss elements of the skins with a cross-sectional area of 10 mm^2.

A significant difference has been observed between the solutions in Figs. 12 and 14. As shown in Fig. 14, material distributions are concentrated around the center of the unit cell. This can be attributed to the reasoning that due to the presence of metal coversheets, the trusses will be more useful in transferring the loads from the inner coversheets to the outer tank wall since the outer coversheet will contain nodes 5, 6, 7 and 8, which are fixed. The members with gray

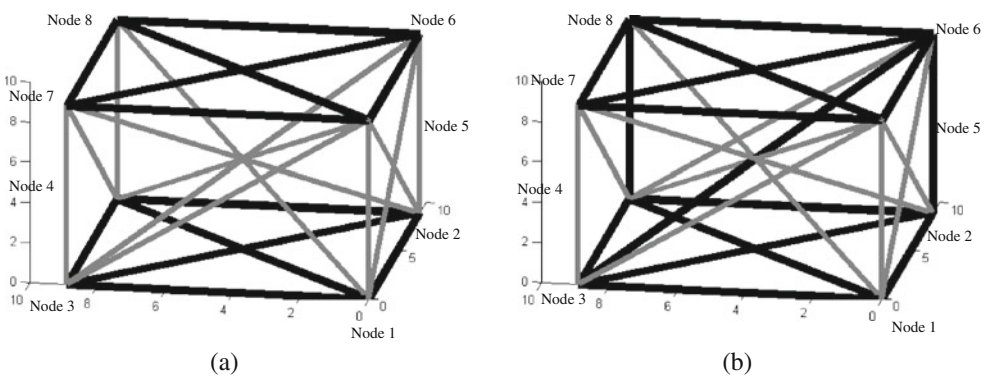

Fig. 14 Optimization solutions considering coversheets for tank. (**a**) Deterministic optimum (**b**) Stochastic optimum using PNN

color represent truss elements with cross-sectional area of 7 mm^2 and black color represents truss elements with cross-sectional area of 10 mm^2. There are 23 truss members in the deterministic solution represented in Fig. 14a, and there are 24 truss members in the stochastic solution represented in Fig. 14b out of which 12 truss members constitute the permanent truss members- representing the inner and outer skins. The truss element connecting node 4 and node 6 is the additional truss element in the stochastic solution. The stochastic optimum is resistant to buckling and has a probability of failure of 8.6×10^{-5} when P_f was evaluated using 1,000,000 samples of LHS. This design method results in a different truss structure configuration where much of the material is distributed in the space within the unit cell. The underlying assumption here is that the inner and outer layer of the wall will be covered with metal sheets which are stiff enough to undergo only negligible deformation when subjected to the boundary conditions that the hydrogen storage tank is being designed for.

5 Conclusion

An exploratory framework that can consider the probabilistic constraints in the design of structural systems has been proposed by integrating the PNN into the conventional topology optimization procedure. In this framework, the PNN played an important role in constructing the classifier for evaluating reliability constraints and LHS was conducted to evaluate P_f with the trained classifier. The effectiveness of the proposed framework was demonstrated with a ground truss example and a practical engineering problem of designing cellular structures for the hydrogen storage tank with the consideration of random field inputs. The applicability of the PNN based classification procedure was also shown to be effective in cases of disjoint failure domain problems, such as topology optimization problems with buckling constraints. Due to the advantage from the selected PNN based classification scheme, the implemented framework can facilitate the quantification of uncertainties in the design of cellular materials which can be highly influenced by nonlinear mechanisms. The result obtained from the proposed method for the case of ground structure was compared with the deterministic optimization result to represent the importance of reliability calculations. A hydrogen storage tank inner lining design example was presented to exemplify the applicability of the proposed procedure for the design of complex products. The hydrogen storage tank inner lining design example problem was solved assuming that the hoop stress and the radial stress remain the same even if the walls of the tank are comprised of truss elements. Buckling phenomenon was absent in the final design obtained for the inner lining which further illustrates the applicability of the proposed framework to practical engineering applications.

References

Atlas L, Cole R et al (1990) Performance comparisons between backpropagation networks and classification trees on three real-world applications. Adv Neural Inf Process Syst 2:622–629

Basudhar A, Missoum S et al (2008) Limit state function identification using Support Vector Machines for discontinous responses and disjoint failure domains. Probab Eng Mech 23:1–11

Brown DE, Corruble V et al (1993) A comparison of decision tree classifiers with backpropagation neural networks for multimodal classification problems. Pattern Recogn 26:953–961

Bendsøe M, Kikuchi N (1988) Generating optimal topologies in structural design using a homogenization method. Comput Methods Appl Mech Eng 71(2):197–224

Bendsøe M, Sigmund O (2003) Topology optimization: theory, methods and applications. Springer, Berlin

Cacoullos T (1966) Estimation of a multivariate density. Ann Math Stat 18(2):179–189

Conti S, Held H, Pach M et al (2008) Shape optimization under uncertainty – A stochastic programming perspective. SIAM J Optim 19(4):1610–1632

Chen S, Chen W, Lee S (2010) Level set based robust shape and topology optimization under random field uncertainties. Struct Multidiscipl Optim 41(4):507–524

Chien YT, Fu KS (1967) On the generalized Karhunen-Loeve expansion. IEEE Trans Inf Theory 13:518–520

Choi S, Grandhi RV et al (2006) Reliability- based design optimization. London, Springer

Chtioui Y, Bertrand D et al (1997) Comparison of multilayer perceptron and probabilistic neural networks in artificial vision. Application to the discrimination of seeds. J Chemom 11(2):111–129

Curram SP, Mingers J (1994) Neural networks, decision tree induction and discriminant analysis: an emperical comparison. J Oper Res Soc 45(4):440–450

Cybenko G (1989) Approximation by superposition of a sigmoidal function. Math Control Signals Syst 2:303–314

Dietterich TG, Bakiri G (1995) Solving multiclass learning problems via error-correcting output codes. J Artif Intell Res 2:263–286

Dobbs MW, Felton LP (1969) Optimization of truss geometry. J Struct Div ASCE 95:2105–2118

Duda PO, Hart PE (1973) Pattern classification and scene analysis. New York, Wiley

Frecker M, Ananthasuresh GK, Nishiwaki S, Kikuchi N, Kota S (1997) Topological synthesis of compliant mechanisms using multi-criteria optimization. ASME J Mech Des 119(2):238–245

Fukunaga K, Koontz WLG (1970) Application of the Karhunen-Loève Expansion to feature selection and ordering. IEEE Trans Comput C-19(4):311–318

Hornik K (1991) Approximation capabilities of multilayer feedforward networks. Neural Netw 4:251–257

Hornik K, Stinchcombe M et al (1989) Multilayer feedforward networks are universal approximators. Neural Netw 2:359–366

Hotelling H (1933) Analysis of a complex of statistical variables into principal components. J Educ Psychol 24:498–520

Huang MS, Lippmann RP (1987) Comparisons between neural net and conventional classifiers. In: IEEE 1st international conference on neural networks. San Diego, CA, pp 485–493

Hurtado JE, Alvarez DA (2003) Classification approach for reliability analysis with stochastic finite-element modeling. J Struct Eng 129(8):1141–1149

Kharmanda G, Olhoff N et al (2004) Reliability-based topology optimization. Struct Multidiscipl Optim 26(5):295–307

Kirsch U (1990) On singular topologies in optimum structural design. Struct Multidiscipl Optim 2:133–142

Kogiso N, Ahn W, Nishiwaki S et al (2008) Robust topology optimization for compliant mechanisms considering uncertainty of applied loads. J Adv Mech Des Syst Manuf 2(1):96–107

Maute K, Frangopol DM (2003) Reliability-based design of MEMS mechanisms by topology optimization. Comput Struct 81(8–11): 813–824

McKay MD, Beckman RJ, Conover WJ (1979) A comparison of three methods for selecting values of input variables in the analysis of output from a computer code. Technometrics 21(2):239–245

Michelle AGM (1904) The limits of economy of materials in frame structures. Philos Mag 8(47):589–597

Michie D, Spiegelhalter DJ et al (1994) Machine learning, neural, and statistical classification. London, UK

Parzen E (1962) On estimation of a probability density function and mode. Ann Math Stat 33:1065–1076

Patel J, Choi S-K (2009) Optimal synthesis of mesostructured materials under uncertainty. In: 50th AIAA/ASME/ASCE/AHS/ASC structures, structural dynamics, and material conference and 5th AIAA multidisciplinary design optimization specialist conference. Palm Springs, CA

Patwo E, Hu MY et al (1993) Two-group classification using neural networks. J Decis Sci 24(4):825–845

Richard MD, Lippmann R (1991) Neural network classifiers estimate Bayesian a posteriori probabilities. Neural Comput 3:461–483

Rozvany GIN, Bendsøe MP, Kirsch U (1995) Layout optimization of structures. Appl Mech Rev 48:41–119

Seepersad CC, Allen JK, McDowell DL, Mistree F (2006) Robust design of cellular materials with topological and dimensional imperfections. Mech Des 128:1285–1297

Sigmund O (1995) Tailoring materials with prescribed elastic properties. Mech Mater 20:351–368

Specht DF (1967) Generation of polynomial discriminant functions for pattern recognition. IEEE Trans Electron Comput EC-16:308–319

Specht DF (1990) Probabilistic neural networks. Neural Netw 3:109–118

Sved G, Ginos Z (1968) Structural optimization under multiple loading. Int J Mech Sci 8:803–805

Tsui KL (1992) An overview of Taguchi method and newly developed statistical methods for robust design. IIE Trans 24(5):44–57

Tu J, Choi KK (1997) A performance measure approach in reliability-based structural optimization. Technical Report R97–02, University of Iowa

Wang Y, Adali T et al (1998) Quantification and segmentation of brain tissues for MR images: a probabilistic neural network approach. IEEE Trans Image Process 7(8):1165–1181

Wang MY, Chen SK, Wang X et al (2005) Design of multi-material compliant mechanisms using level set methods. ASME J Mech Des 127(5):941–956

Witten IH, Frank E (2005) Data mining: practical machine learning tools and techniques. Morgan Kauffman Publications, San Francisco

Zhang GP (2000) Neural networks for classification: a survey. IEEE Trans Syst Man Cybern C Appl Rev 30(4):451–462

Zhou M (1996) Difficulties in truss topology optimization with stress and local buckling constraints. Struct Multidiscipl Optim 11:134–136